Low-Temperature, Solution-Processed MoO x for Efficient and Stable Organic Solar Cells

5 AUTHORS, INCLUDING:

Kirill Zilberberg
Bergische Universität Wuppertal
23 PUBLICATIONS   **556** CITATIONS

SEE PROFILE

Andreas Behrendt
Bergische Universität Wuppertal
19 PUBLICATIONS   **267** CITATIONS

SEE PROFILE

Sara Trost
Bergische Universität Wuppertal
20 PUBLICATIONS   **335** CITATIONS

SEE PROFILE

Low-Temperature, Solution-Processed MoO$_x$ for Efficient and Stable Organic Solar Cells

Kirill Zilberberg, Houssem Gharbi, Andreas Behrendt, Sara Trost, and Thomas Riedl*

Institute of Electronic Devices, University of Wuppertal, Rainer-Gruenter-Strasse 21, 42119 Wuppertal, Germany

S Supporting Information

ABSTRACT: Sol−gel processed MoO$_x$ (sMoO$_x$) hole-extraction layers for organic solar cells are reported. A Bis(2,4-pentanedionato)molybdenum(VI)dioxide/isopropanol solution is used and only a moderate thermal post deposition treatment at 150 °C in N$_2$ ambient is required to achieve sMoO$_x$ layers with a high work-function of 5.3 eV. We demonstrate that in P3HT:PC$_{60}$BM organic solar cells (OSCs) our sMoO$_x$ layers lead to a high filling factor of about 65% and an efficiency of 3.3% comparable to that of reference devices with thermally evaporated MoO$_3$ layers (eMoO$_3$). At the same time, a substantially improved stability of the OSCs compared to devices using a PEDOT:PSS hole extraction layer is evidenced.

KEYWORDS: organic solar cell, high work-function materials, sol−gel metal oxides, transition metal oxides, stability, PEDOT:PSS
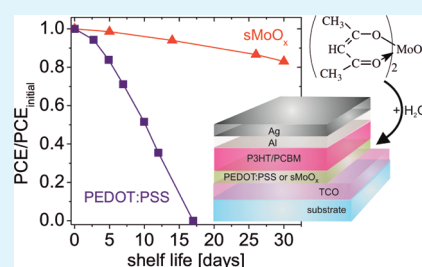
The cost-effective large-scale manufacturing of organic solar cells (OSCs) via printing techniques requires the processing of all layers in the device from liquid phase. A substantial amount of work has been devoted to the solution processing of the active donor/acceptor blend which is frequently used in so-called bulk-heterojunction (BHJ) devices. Aside from that, modern highly efficient OSCs incorporate functional interlayers next to the electrodes which facilitate the extraction of the photogenerated charges. At the anode side, polyethylene dioxythiophene:polystyrene sulfonate (PEDOT:PSS) casted from an aqueous dispersion is routinely used. However, substantial device instability has been associated with the acidic nature of PEDOT:PSS and the residual water typically present in the layers.[1−5]

On the other hand, transition metal oxides (TMOs) like V$_2$O$_5$, WO$_3$, MoO$_3$ with a high work-function (WF) up to 7 eV have successfully been used to replace PEDOT:PSS.[6−11] In most cases, these TMO layers are prepared via thermal evaporation.[12] Very recently, we introduced a sol−gel process for V$_2$O$_5$ layers which without any post-treatment replaced PEDOT:PSS in OSCs and concomitantly led to an improved device lifetime.[13,14] A slight drawback of V$_2$O$_5$ is the relatively low band gap of around 2.3 eV, which for thicker layers (>10 nm) may cause substantial absorption losses in the spectral region relevant for organic solar cells. From this point of view, MoO$_3$ with a larger band gap of 2.9 to 3.1 eV[15,16] could be preferable.

Solution processing of MoO$_3$ is currently pursued by various groups. Recently, Meyer et al. prepared MoO$_3$ layers by using MoO$_3$ nanoparticles (NPs) with a polymer as dispersing agent.[17] After deposition, the layers had to be thermally annealed at 100 °C and a subsequent oxygen plasma treatment was required to remove the polymer dispersant. A high WF of the resulting layers of 5.7−6 eV has been obtained. Aside from the post processing requirements, a substantial drawback of the

approach is the formation of larger NP aggregates with a size of 100 nm and an overall high layer roughness of 25 nm (rms). Because of their roughness, these NP layers may be critical sources of short circuit faults especially on a large device area. Another approach is the preparation of MoO$_x$ from a sol−gel process.[18,19] In the sol−gel approach reported by Girotto et al., postdeposition annealing at elevated temperatures (at least 275 °C) was required for the full formation of MoO$_x$ layers and in order to achieve reasonable device efficiencies. This high-temperature annealing is problematic if common polymer substrates are to be used. In the sol−gel process reported by Liu et al., larger particle aggregates and discontinuous MoO$_x$ layers have been found, limiting the applicability of the process.

In this work, we report BHJ OSCs based on poly(3-hexylthiophene): [6,6]-phenyl-C$_{61}$-butyric acid methyl ester (P3HT:PCBM) with sol−gel processed MoO$_x$ hole extraction layers prepared from a Bis(2,4-pentanedionato)molybdenum-(VI)dioxide/isopropanol solution. MoO$_x$ layers formed via hydrolysis reaction at room temperature in ambient air. Only a moderate thermal post-treatment at 150 °C in N$_2$ ambient is required to achieve MoO$_x$ layers with a high WF of 5.3 eV. It is found that the annealing step is necessary to remove adsorbates from the MoO$_x$ surface. We demonstrate that the use of our sMoO$_x$ layers in OSCs yields a high filling factor of about 65% and an efficiency of 3.3% comparable to that of reference devices with thermally evaporated MoO$_3$ layers (eMoO$_3$). At the same time, a substantially improved stability of the OSCs compared to reference devices using a PEDOT:PSS hole extraction layer is evidenced.

■ EXPERIMENTAL SECTION

The polymer-fullerene OSCs studied in this work have the following layer sequence glass/ITO/(sMoO$_x$ or eMoO$_3$ or PEDOT:PSS)/P3HT:PC$_{60}$BM/Al/Ag with an active area of 0.03 cm^2. The MoO$_x$ layers were spin-coated from isopropanol (containing about 0.1% of H$_2$O) solution of Bis(2,4-pentanedionato)molybdenum(VI)dioxide (TCI Europe) at 1:150 w/v ratio. The layers were subsequently kept at ambient air for 1 h for hydrolysis. As a reference, devices with PEDOT:PSS (25 nm) and eMoO$_3$ (20 nm) were used. The PEDOT:PSS (Clevios P VP. AI4083) was spin coated and subsequently annealed for 1 h at 110 °C in ambient atmosphere. For the thermal evaporation of MoO$_3$ in high-vacuum, MoO$_3$ powder (Alfa Aesar) was used in an effusion cell with a boron-nitrite crucible (base pressure 10^{-7} mbar, cell temperature 620 °C and rate 0.04 nm/s). After evaporation, the eMoO$_3$ layers were transferred via ambient air to the glovebox for preparation of the organic layers. The polymer:fullerene blend of P3HT (supplied by Honeywell Chemicals Seelze) and PC$_{60}$BM (American Dye Source Inc.) with a weight ratio of 1:1 was spin-coated under N$_2$ atmosphere from a chlorobenzene and chloroform (vol. ratio 1:1) solution (16 mg mL^{-1}) resulting in an active layer with thickness of 220 nm. Subsequently, the cathode has been thermally evaporated as a bilayer of Al (20 nm) and Ag (100 nm) using a shadow mask. The XPS-spectra were measured in a commercial spectrometer (ESCALAB 5, VG Scientific). All XPS spectra (photoelectron takeoff normal to the surface) were acquired in the constant analyzer energy mode with a pass energy of 20 eV and excitation by nonmonochromatized Mg K−Kα radiation (hν = 1253.6 eV) with an input power of 200 W (10 kV, 20 mA). The quantitative evaluation of the measured XPS signals included a background subtraction according to Shirley[20] and a peak deconvolution with least-squares fit routines.[21] The peak area was weighted with the respective photoionization cross sections published by Scofield.[22]

Further characterization methods used in this work are detailed in the Supporting Information.

■ RESULTS AND DISCUSSION

Bis(2,4-pentanedionato)molybdenum(VI)dioxide has been used to prepare MoO$_x$ layers mainly for catalytic or electrochromic applications. There, high-temperature processing (300−500 °C) is routinely applied in order to achieve specific microstructures or crystalline phases in the material, as required by the particular application.[23,24] As we target substantially lower processing temperatures, preferably room-temperature, it is of importance to study the morphology and composition of the thus resulting layers. As determined by dynamic light scattering (DLS), we found particles with a size of about 1 nm forming in the as-prepared precursor solution which remain stable in size even after stirring the solution in ambient air for at least 30 min. Details about the study of the particle formation in the precursor solution using DLS is provided in the Supporting Information.

The AFM topography of the sMoO$_x$ films reveals a smooth surface (roughness rms <3 nm, see Figure S1a in the Supporting Information), in contrast to typically rough layers obtained from casted MoO$_3$ NP dispersions.[17] In addition, as verified by XRD, the resulting sMoO$_x$ layers are amorphous. There are some voids in the layers, which likely result from the evaporation of the solvent. Voids in sol−gel prepared thin films are commonly found. For example, Orignac et al. have reported an in-depth study of the void formation in sol−gel titania/silica layers spin-coated with ethanol as a solvent. The void formation was linked to the spin-coating process and the evaporation of the solvent.[25] In a further report, Capellani et al. have studied void formation in sol−gel Ta$_2$O$_5$ layers. There, a volume fraction of the voids in as-spun layers as high 30% was evidenced.[26]

XPS analysis of the pristine layers shows that the Mo atoms are mainly in the Mo^{6+} oxidation state (Mo 3d5/2 and Mo 3d3/2 peaks at 232.2 and 235.4 eV, respectively, see Figure 1).
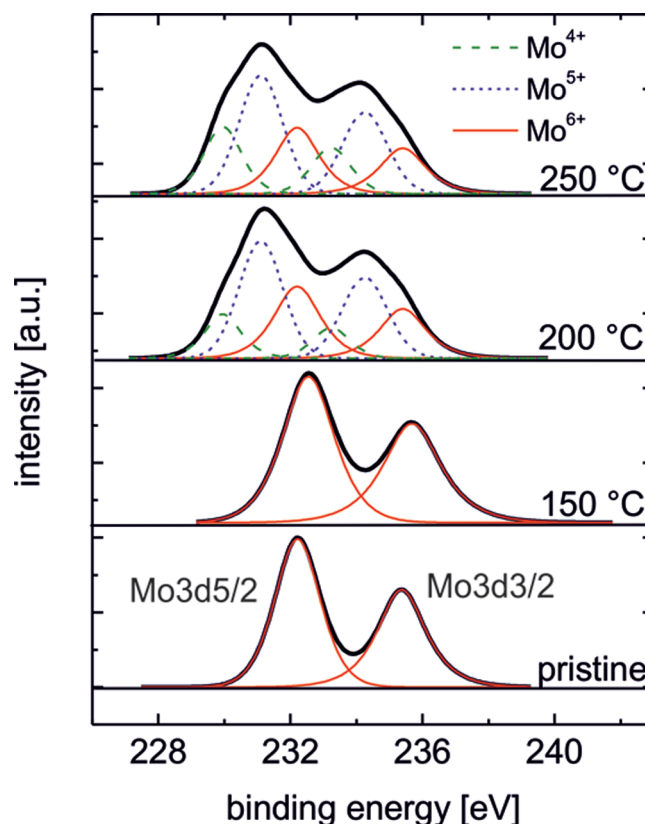

Figure 1. XPS spectra (Mo3d5/2 and Mo3d3/2 peaks) of a pristine sMoO$_x$ layer and sMoO$_x$ layers annealed in N$_2$ atmosphere for 20 min. The spectra have been normalized and vertically offset.

By careful analysis of the C 1s peaks between 285.7 and 286.8 eV, we found a signal due to C−C bonds and due to carbon with single and double bonds to oxygen. As these bonds are also characteristic for the metal−organic precursor used in our process, we cannot separate the signal originating from adsorbates because of air exposure from the signal due to unreacted precursor molecules in the layers. Overall, an upper limit for the ratio of residual carbon atoms to all atoms (Mo, O and C) in the layers can be estimated to 29%. In contrast, for the neat precursor molecule (MoO$_2$(acac)$_2$) about 60% of all atoms (excluding hydrogen) would be carbon atoms. Therefore, we have strong evidence of substantial decomposition of the precursor via hydrolysis even at room temperature. The ratio of the (cross-section-weighted) signal intensities of oxygen vs molybdenum signal is calculated to 2.9 (it would equal 6 for neat nonreacted precursor molecules).

Using these sMoO$_x$ layers as replacement for PEDOT:PSS, we prepared conventional OPV devices (layer sequence see

Figure 2a). To this end, the ITO anode has been coated with pristine a $sMoO_x$ layer with a thickness of 22 nm before
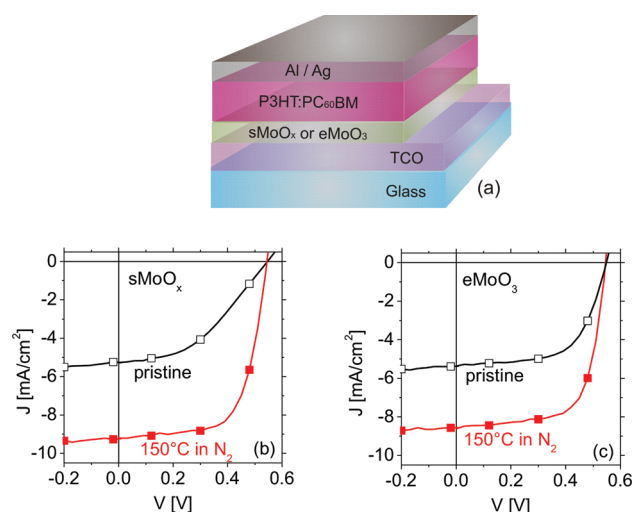

Figure 2. (a) Layer sequence of the solar cells used in this study. J/V characteristics of P3HT:PCBM devices with (b) $sMoO_x$ and (c) $eMoO_3$ hole extraction layers prepared with or without postdeposition annealing in N_2 for 20 min.

deposition of the organic BHJ. The resulting cells show a poor power conversion efficiency (PCE) of 1.3% mainly limited due to a low J_{sc} and FF (Figure 2b, Table 1). It is important to note,

Table 1. Characteristics of $sMoO_x$ (22 nm) Devices Dependent on Treatment Procedure before the Deposition of BHJ[a]

	PCE (%)	V_{oc} (V)	J_{sc} (mA/cm^2)	FF(%)
$sMoO_x$ pristine	1.3	0.54	5.3	44.5
$sMoO_x$, annealed 20 min at 150 °C in N_2	**3.3**	**0.54**	**9.2**	**65.5**
PEDOT:PSS - control device	3.2	0.56	9.8	57.9
$eMoO_3$ pristine	1.8	0.55	5.4	61.2
$eMoO_3$, annealed 20 min at 150 °C in N_2	**3.2**	**0.55**	**8.6**	**67.6**

[a]The characteristics of optimized control devices based on PEDOT:PSS and $eMoO_3$ (20 nm) hole extraction layers are given for comparison.

that control devices with air-exposed $eMoO_3$ demonstrated a similarly low J_{sc} of 5 mA/cm^2 (Figure 2c, Table 1).

Kelvin probe analysis of the pristine $sMoO_x$ layers gave a surprisingly low WF of 4.9 eV, despite the fact that the WF of fresh $eMoO_3$ has been derived to be 6.9 eV.[9] In previous reports, it has been found that air exposure substantially lowers the WF of TMO layers because of adsorbates at the surface.[6,15] To remove potential adsorbates from the surface of our samples, both $sMoO_x$ and $eMoO_3$ were postannealed in a N_2 atmosphere for 20 min at 150 °C before deposition of the organic active layer. As a result, the WF increased from 4.9 to 5.3 eV (ΔWF = 0.4 eV, a similar ΔWF was found for air-exposed $eMoO_3$ after annealing in N_2). Concomitantly, a dramatic improvement of the OSCs fabricated on top of these annealed layers was found (J_{sc} to 9.2 mA/cm^2 and FF to 65.5%) (Figure 2, Table 1). Both, $sMoO_x$ and $eMoO_3$ devices show essentially comparable device characteristics with a PCE of

3.3%. It is important to note, that the layer morphology of the $sMoO_x$ remains unaffected by this annealing process (see Figure S1b in the Supporting Information).

To further support our conclusion that the main function of the annealing step in N_2 atmosphere is the removal of adsorbates from the surface of the $sMoO_x$ layer, we annealed a layer of $sMoO_x$ in N_2 but subsequently exposed it to ambient air (to allow for the formation of adsorbates) before retransfering it to the glovebox for deposition of the BHJ. As for the devices with a neat $sMoO_x$ layer, a substantial drop in J_{sc} (8.1 mA/cm^2) and FF (56.4%) is found (J/V curve not shown here).

We found that annealing of the MoO_x layers in N_2 for 20 min between 130 and 150 °C results in optimum device characteristics (Figure 3). These moderate post processing
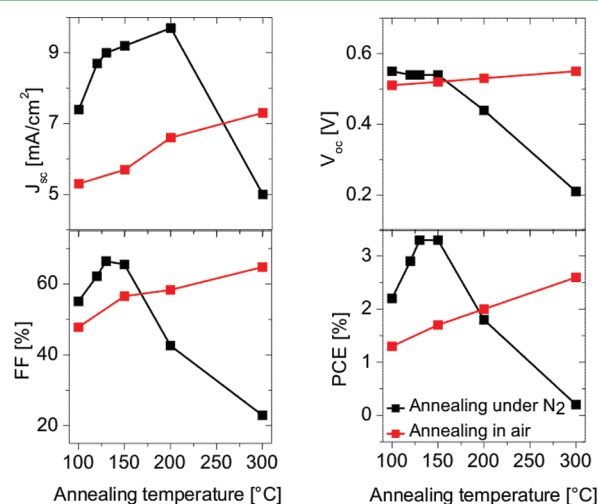

Figure 3. Characteristics of OSCs with a $sMoO_x$ layer (22 nm) layer annealed in air and N_2, respectively, at various temperatures previous to the deposition of the organic BHJ.

temperatures are especially favorable for temperature sensitive substrates. Annealing at 150 °C in excess of 20 min does not lead to a further improvement (see Figure S4 in the Supporting Information). Annealing at higher temperatures leads to a rapid drop of V_{oc}, FF, J_{sc}, and PCE (Figure 3).

It is interesting to study the change of the optical properties of the $sMoO_x$ layers upon thermal treatment. A reduction of the band gap of neat $sMoO_x$ from 2.76 to 2.4 eV is found upon annealing at 200 °C (see Figure S3 in the Supporting Information). Concomitantly, the sub-bandgap absorption increases, which hints to an increased formation subgap states in the $sMoO_x$. This behavior is associated with an increased formation of Mo^{5+} species and is known as thermochromism of molybdenum oxide.[27,28] This thermochromic behavior is accompanied by an increase of electrical conductivity of the $sMoO_x$ by an order of magnitude and a slightly reduced WF (5.1 eV) upon annealing at 200 °C in N_2 as compared to 150 °C (see Table S1 in the Supporting Information).

Figure 1 shows XPS spectra of $sMoO_x$ annealed in N_2 at varied temperatures in comparison to a pristine $sMoO_x$ layer. Although there is no substantial change of the Mo3d5/2 and Mo3d3/2 peaks up to 150 °C, for higher annealing temperatures we observe strong contributions toward lower binding energies which can be related to the formation of Mo^{5+} and Mo^{4+}. As has recently been shown, these reduced Mo species

1166

dx.doi.org/10.1021/am201825t | ACS Appl. Mater. Interfaces 2012, 4, 1164–1168

account for the formation of gap states in MoO_x.[29] A similar finding has recently been published for V_2O_5.[6] This is in-line with the increased subgap absorption we have discussed above. The increased number of gap states may add to parasitic recombination of photogenerated charge carriers close to the interface $sMoO_x$/organic which would result in a decay of the FF, as observed in Figure 3 for $T > 150$ °C.[30]

On the contrary, the OSCs with $sMoO_x$ layers annealed in ambient air show a different behavior. As is demonstrated, even after annealing at 300 °C a continuous increase of V_{oc}, J_{sc}, and FF is seen (Figure 3). Note, the performance of the $sMoO_x$ layers annealed in ambient air is limited by the reformation of adsorbates upon cooling of the sample before transfer to the N_2 glovebox for deposition of the BHJ.

As a result of the optimization discussed above, we have used $sMoO_x$ layers annealed at 150 °C in N_2 for 20 min for our further experiments. To analyze the impact of $sMoO_x$ layer thickness on the device performance we have varied the $sMoO_x$ layer thickness from 10 to 52 nm (Table 2). We found an

Table 2. Characteristics of OSCs with Varied $sMoO_x$ Layer Thickness

$sMoO_x$ layer thickness(nm)	PCE (%)	V_{oc} (V)	J_{sc} (mA/cm^2)	FF (%)
10	3.1	0.55	9.1	62.7
22	3.3	0.54	9.2	65.5
30	2.9	0.54	8.9	59.4
52	2.9	0.55	8.3	64.3

optimum layer thickness of 22 nm. Because of the voids observed in the AFM measurements above, thinner layers may cause an incomplete coverage of the ITO surface, resulting in less efficient hole-extraction from P3HT. For devices with thicker MoO_x layers, the slight drop of J_{sc} can be explained by an increase in optical absorption losses. For instance, the 52 nm thick $sMoO_x$ layer transmits about 7% less light compared to that with the optimized thickness of 22 nm. This has been estimated by integration of the transmitted light of the solar simulator in the range of 350 to 650 nm (absorption band of P3HT:PC_{60}BM). However, for comparison, a 52 nm thick layer of sol−gel processed V_2O_5, which has a substantially smaller bandgap than $sMoO_x$, would cause about twice as high absorption losses in the same spectral region.[13] Other than J_{sc}, the FF does not show a significant change upon variation of the $sMoO_x$ layer thickness. The somewhat lower value of FF for the 30 nm device is within the statistical variation of the experiment.

As discussed in the introduction, PEDOT:PSS may lead to substantial device instabilities in OSCs, which is an important motivation to replace PEDOT:PSS with a TMO hole-extraction layer. Remarkably, as shown in Figure 4, the use of a $sMoO_x$ layer instead of PEDOT:PSS allows for substantially increased device stability for devices stored in N_2 and ambient air (45−60% RH), respectively. After 30 days, the PEDOT:PSS devices stored in N_2 drop to about 58% of the initial PCE, whereas the devices stored in ambient air fail entirely. The observed decrease of the PCE in all cases is mainly due to a deterioration of both J_{sc} and FF, in agreement with previous studies.[13] Stability issues related to the use of PEDOT:PSS as interlayer at the anode have been discussed in a very recent review by Krebs et al.[31] In spite of a plethora of reports on this topic, the particular reasons of device instability owing to PEDOT:PSS are still under debate. In agreement with our observation,
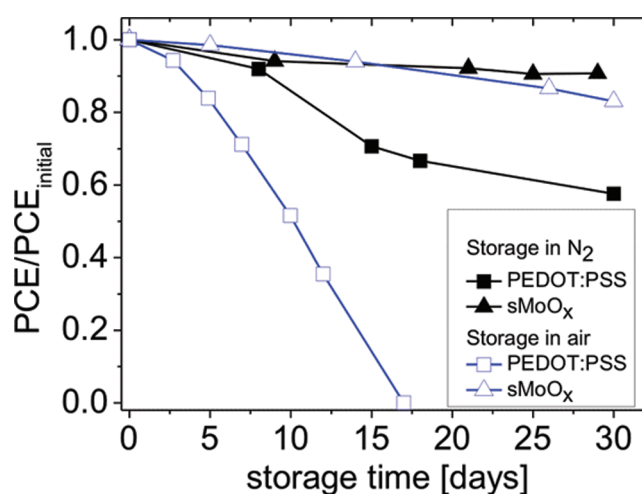

Figure 4. Long-term stability of the PCE of OSCs based on either PEDOT:PSS or $sMoO_x$ hole extraction layers. The devices have been stored in N_2 and ambient air (rel. humidity in a range of 44−62%), respectively.

Voroshazi et al. have recently studied the degradation of OSCs based on PEDOT:PSS which was found to occur even under inert atmosphere.[32] In this report, residual moisture in the PEDOT:PSS, which causes corrosion of the cathode layer was proposed as a possible reason for the degradation observed. A similar mechanism may be responsible for the decay of our PEDOT:PSS-based devices in an inert atmosphere.

On the contrary, the devices with $sMoO_x$ are found to show dramatically improved stability and after 30 days retain 90% of their initial PCE in N_2 and 84% in air (Figure 4). This is in excellent agreement with the stability of OSCs using thermally evaporated MoO_x layers. Voroshazi et al., have reported the stability behavior of P3HT:PCBM cells comprising a thermally evaporated MoO_x layer under varied ambient humidity.[33] After 600 h in ambient air (35%rh), the PCE dropped to 80% of its initial value. We can therefore conclude that our solution-processed $sMoO_x$ layers allow for OSCs with a long-term stability comparable to that based on evaporated MoO_x.

■ CONCLUSIONS

We introduced an efficient low-temperature sol−gel process for the MoO_x charge extraction layer for organic solar cells. Only a moderate thermal post treatment at 130−150 °C in N_2 ambient is required to achieve MoO_x layers with a high WF of 5.3 eV. It is shown that the annealing step is necessary to remove adsorbates from the MoO_x surface. It is shown that in optimized devices the use of $sMoO_x$ layers yields a high filling factor of about 65% and an efficiency of 3.3% comparable to that of reference devices with thermally evaporated MoO_3 layers. At the same time a substantially improved stability of the OSCs compared to reference devices using a PEDOT:PSS hole extraction layer is evidenced.

■ ASSOCIATED CONTENT

Ⓢ Supporting Information
Characterization techniques for layers and devices; molecular structure of the precursor used; AFM data, XPS data, Tauc's plots for $sMoO_x$ and $eMoO_3$ layers; plot of OSC characteristics as a function of annealing time; table with electrical conductivity data. This material is available free of charge via the Internet at http://pubs.acs.org/.

■ AUTHOR INFORMATION

Corresponding Author
*E-mail: t.riedl@uni-wuppertal.de.

Notes
The authors declare no competing financial interest.

■ REFERENCES

(1) Pingree, L. S. C.; MacLeod, B. A.; Ginger, D. S. *J. Phys. Chem. C* **2008**, *112*, 7922.

(2) Hau, S. K.; Yip, H. L.; Zou, J. Y.; Jen, A. K. Y. *Org. Electron.* **2009**, *10*, 1410.

(3) So, F.; Kondakov, D. *Adv. Mater.* **2010**, *22*, 3762.

(4) De Jong, M. P.; Van Ijzendoorn, L. J.; De Voigt, M. J. A. *Appl. Phys. Lett.* **2000**, *77*, 2255.

(5) Jorgensen, M.; Norrman, K.; Krebs, F. C. *Sol. Energy Mater. Sol. Cells* **2008**, *92*, 686.

(6) Meyer, J.; Zilberberg, K.; Riedl, T.; Kahn, A. *J. Appl. Phys.* **2011**, *110*, 033710.

(7) Schmidt, H.; Flügge, H.; Winkler, T.; Bülow, T.; Riedl, T.; Kowalsky, W. *Appl. Phys. Lett.* **2009**, *94*, 243302.

(8) Meyer, J.; Hamwi, S.; Bülow, T.; Johannes, H. H.; Riedl, T.; Kowalsky, W. *Appl. Phys. Lett.* **2007**, *91*, 113506.

(9) Kröger, M.; Hamwi, S.; Meyer, J.; Riedl, T.; Kowalsky, W.; Kahn, A. *Appl. Phys. Lett.* **2009**, *95*, 123301.

(10) Kröger, M.; Hamwi, S.; Meyer, J.; Riedl, T.; Kowalsky, W.; Kahn, A. *Org. Electron.* **2009**, *10*, 932.

(11) Li, G.; Chu, C.-W.; Shrotriya, V.; Huang, J.; Yang, Y. *Appl. Phys. Lett.* **2006**, *88*, 253503.

(12) Meyer, J; Winkler, T.; Hamwi, S.; Schmale, S.; Johannes, H.-H.; Weimann, T.; Hinze, P.; Kowalsky, W.; Riedl, T. *Adv. Mater.* **2008**, *20*, 3839−3843.

(13) Zilberberg, K.; Trost, S.; Schmidt, H.; Riedl, T. *Adv. Energy Mater.* **2011**, *1*, 377−381.

(14) Zilberberg, K.; Trost, S.; Meyer, J.; Kahn, A.; Behrendt, A.; Lützenkirchen-Hecht, D.; Frahm, R.; Riedl, T. *Adv. Funct. Mater.* **2011**, *21*, 4776.

(15) Meyer, J.; Shu, A.; Kröger, M.; Kahn, A. *Appl. Phys. Lett.* **2010**, *96*, 133308.

(16) Shrotriya, V.; Li, G.; Yao, Y.; Chu, C.-W.; Yang, Y. *Appl. Phys. Lett.* **2006**, *88*, 073508.

(17) Meyer, J.; Khalandovsky, R.; Görrn, P.; Kahn, A. *Adv. Mater.* **2011**, *23*, 70.

(18) Girotto, C.; Voroshazi, E.; Cheyns, D.; Heremans, P.; Rand, B. P. *ACS Appl. Mater. Interfaces* **2011**, *3* (9), 3244−3247.

(19) Liu, F.; Shao, Sh.; Guo, X.; Zhao, Y.; Xie, Zh. *Sol. Energy Mater. Sol. Cells* **2010**, *94*, 842−845.

(20) Shirley, D. A. *Phys. Rev. B* **1972**, *5*, 4709.

(21) Wojdyr, M. *J. Appl. Crystallogr.* **2010**, *43*, 1126.

(22) Scofield, J. H. *J. Electron Spectrosc.* **1976**, *8*, 129.

(23) Mallikarjuna, N. N.; Venkataraman, A. *J. Therm. Anal. Calorim.* **2002**, 901−907.

(24) Jiebing, S.; Rui, X.; Shimin, W.; Wufeng, T.; Hua, T.; Jing, S. *J. Sol−Gel Sci. Technol.* **2003**, *27*, 315−319.

(25) Orignac, X.; Vasconcelos, H. C.; Du, X. M.; Almeida, R. M. *J. Sol−Gel Sci. Technol.* **1997**, *8*, 243−248.

(26) Cappellani, A.; Keddie, J. L.; Barradas, N. P.; Jackson, S. M. *Solid-State Electron.* **1999**, *43*, 1095.

(27) Boudaoud, L.; Benramdane, N.; Desfeux, R.; Khelifa, B.; Mathieu, C. *Catal. Today* **2006**, *113*, 230−234.

(28) Quevedo-Lopez, M. A.; Reidy, R. F.; Orozco-Teran, R. A.; Mendoza-Gonzalez, O.; Ramirez-Bon, R. *J. Mater. Sci.: Mater. Electron.* **2000**, *11*, 151−155.

(29) Vasilopoulou, M.; Palilis, L. C.; Georgiadou, D. G.; Kennou, S.; Kostis, I.; Davazoglou, D.; Argitis, P. *Appl. Phys. Lett.* **2012**, *100*, 013311.

(30) Street, R. A.; Schoendorf, M.; Roy, A.; Lee, J. H. *Phys. Rev. B* **2010**, *81*, 205307.

(31) Jorgensen, M.; Norrman, K.; Gevorgyan, S. A.; Tromholt, T.; Andreasen, B.; Krebs, F. C. *Adv. Mater.* **2012**, *24*, 580−612.

(32) Voroshazi, E.; Verreet, B.; Aernouts, T.; Heremans, P. *Solar Energy Mater. Solar Cells* **2011**, *95*, 1303−1307.

(33) Voroshazi, E.; Verreet, B.; Buri, A.; Müller, R.; Nuzzo, D. D.; Heremans, P. *Org. Electron.* **2011**, *12*, 736−744.